Hydrothermal Preparation of *Phyllostachys pubescens* – nanocellulose/Graphene Aerogel as a Simple Device for Supercapacitors

Yan-Yun Wang, Qing-Jin Fu, Xiao Ning, Ge-Gu Chen, and Chun-Li Yao *

Bamboo nanocellulose can be regarded as a promising biomass material for the preparation of sustainable energy devices due to its unique structure, excellent properties, and wide range of sources. A highly conductive electrochemical energy storage was synthesized due to the excellent electrical conductivity of graphene and the high surface area of nanocellulose and graphene, which was beneficial for producing a network structure. The symmetric capacitor assembled from the *Phyllostachys pubescens* nanocellulose/graphene aerogel (CGA) electrode exhibited a high specific capacitance of 125.5 F/g at 5 mV/s and extreme stability of 98.3% capacitance retention ratio after 5000 cycles at 2 A/g. This nanocellulose-graphene electrode showed potential for future high-performance supercapacitors.

Keywords: Nanocellulose; Sustainables; Supercapacitors; Graphene oxide; Aerogel

*Contact information: Beijing Key Laboratory of Lignocellulosic Chemistry, Beijing Forestry University, Beijing 100083, China; *Corresponding author: chunliyao2006@163.com*

INTRODUCTION

Supercapacitors, as electrochemical capacitors, can be regarded as the most promising energy storage devices. They have received increased attention because of their high power density, high charging/discharging rate capability, excellent reversibility, and long cycling life (Lei *et al.* 2016). Supercapacitors can be classified into electrochemical double-layer capacitors (EDLC) and pseudocapacitors based on different charge mechanisms. The capacitance of EDLCs relies on electrostatic charge diffusion and adsorption between the surface of the electrode and electrolyte solution (González *et al.* 2016). Carbon materials, such as activated graphene (Zhu *et al.* 2011), carbon nanotubes (CNTs) (Izadi‐Najafabadi *et al.* 2010), mesoporous carbons (Sun *et al.* 2012), and carbide-derived carbons (Merlet *et al.* 2012), as a kind of EDLC electrode material, can provide efficient charge separation in electrolyte solutions and enhance the overall electron transport efficiency in the electrode (Li *et al.* 2016). In recent years, there has been an increasing interest in combining two carbon materials, such as graphene and activated carbons (ACs) (Xu *et al.* 2015; Yu *et al.* 2014), graphene and CNTs (Saeed *et al.* 2018), or carbon nanofibers and ACs (Gryglewicz *et al.* 2013), to improve the electrochemical properties of materials. However, the composites with two carbon materials usually do not achieve the desired results because of the lack of affinity between the different carbon materials, which results in a poor distribution and aggregation of the same material (Du *et al.* 2017).

Cellulose is the most abundant renewable natural polysaccharide (Titirici *et al.* 2012). Nanocellulose derived from cellulose is one of the most promising sustainable

nanomaterials (Dufresne 2013). Nanocellulose has a high aspect ratio, excellent mechanical properties, impressive flexibility, and excellent hydrophilicity, making it easy to assemble carbon materials into flexible, adhesive-free, and high-performance electrodes (Okita *et al.* 2010; Saito *et al.* 2006). Wang *et al.* (2013) prepared a core-sheath conductive nanocomposite with excellent conductivity of 77 $S \cdot cm^{-1}$ (Zhang *et al.* 2019). Wu *et al.* (2014) developed a core-shell PPy / PVP / CNC conductive material with high conductivity of 36.9 $S \cdot cm^{-1}$ and excellent specific capacitance of 322.6 $F \cdot g^{-1}$, and improved cycle stability. Zhou *et al.* (2013) used graphite nanosheets (GNPs) to insert bacterial cellulose (BC) to increase the electrical conductivity of the composite membrane and obtain a maximum conductivity of 1.2 $S \cdot m^{-1}$. Feng *et al.* (2012) proposed a highly flexible nanocomposite film of bacterial cellulose (BC) and graphene oxide (GO) with flexible structure by vacuum assisted self-assembly technology. The conductivity of the composite film containing 1 wt% GO after in situ reduction showed a significant increase of 6 orders of magnitude compared with the insulated BC. Park *et al*. (2016) prepared a unique conductive bacterial cellulose (BC) composite with silicon nanoparticles (SiNPs) and polyaniline, which achieved very stable electrical conductivity even after repeated bending for more than 100 times. Furthermore, nanocellulose possesses a hydroxyl-containing reactive surface that can be beneficial for the contact between the electrodes and electrolytes as well as to enhance the electrochemical performance of the electrodes (Chen *et al.* 2018).

In this work, the authors prepared nanocellulose from *Phyllostachys pubescens* as a raw material, and a lightweight porous flexible supercapacitor (nanocellulose/graphene aerogel, CGA) based on nanocellulose and graphene oxide was prepared by a green hydrothermal method. In the graphene-nanocellulose aerogel electrode, nanocellulose can effectively avoid the aggregation between graphene sheets and form a stable 3D network structure with graphene oxide, which not only enhances the flexibility of the composite electrode, but also solves the ion diffusion problem caused by the aggregation of graphene sheets (Gao *et al.* 2013). In particular, two important factors, the reaction temperature and the ratio of nanocellulose to graphene, were suitably optimized. The prepared CGA exhibits a good diffusion channel, a rich reaction site for electrostatic attraction and molecular migration, and allows electrolyte ions to be continuously and stably transported to the surface, which leads to an excellent electrochemical performance. The CGA not only has extensive application prospects in flexible energy devices, such as supercapacitors, but also improves the high value application of bamboo cellulose.

EXPERIMENTAL

Materials

Preparation of graphene oxide (GO)

The GO was prepared by a chemical treatment of exfoliated natural graphite powders (Qingdao Chenglong Graphite Co., Ltd., Qingdao, China) according to the modified method of Hummers, Jr. and Offeman (Hummers Jr and Offeman 1958). The final concentration of GO dispersion was 6.3 mg/mL. The GO dispersion was further diluted to 2 mg/mL by adding deionized water.

Preparation of cellulose nanofibers (CNFs)

The cellulose extraction and purification of *Phyllostachys pubescens* and CNF preparation methods were referred to in the literature (Chen *et al.* 2011; Isogai *et al.* 2011). First, the bamboo powder was subjected to solvent extraction with a toluene/ethanol (2:1) (toluene, Fortuneibo-Tech Co., Ltd., Shanghai, China; ethanol, Fujian Zhonghe Environmental Protection Technology Co., Ltd., Fujian, China) mixture for 6 h. Next, the sample was subjected to delignification treatment at 75 °C for 1 h with an acidified sodium chlorite solution (Jinan Huijinchuan Trading Co., Ltd., Shandong, China), and the process was repeated seven times. Then, the sample was treated with 2 wt% potassium hydroxide (Zhengzhou Shuangchen Trading Co., Ltd., Henan, China) at 90 °C for 2 h to remove hemicellulose and obtain highly purified cellulose. Finally, it was treated with a 1 wt% hydrochloric acid solution (Jining Huicheng Huagong Co., Ltd., Shandong, China) at 80 °C for 2 h to obtain cellulose fibers.

The above cellulose fibers (2 g) were suspended in a solution (200 mL) that contained 2,2,6,6-tetramethylpiperidine-N-oxyl (TEMPO) (0.032 g) (Guangzhou Hu'ao Chemical Co., Ltd., Guangdong, China) and sodium bromide (0.2 g) (He'nan Dingjing Chemical Products Co., Ltd., He'nan, China). The cellulose fibers were oxidized by adding the NaClO solution (10 mmol/g cellulose) (Jinan Huijinchuan Trading Co., Ltd., Shandong, China) for 6 h. The pH of the reaction solution was maintained at 10 by adding 0.5 M NaOH (Jiaxiang Sea Chemical Co., Ltd., Shandong, China) during the reaction at 10 °C. The 1 wt% oxidized cellulose/water slurries were ultrasonicated for 30 min at a power of 500 W in an ice bath. Finally, the sample was washed with distilled water to a neutral pH and stored at 4 °C.

Preparation of CGA

The GO (2 mg/mL, 15 mL) and CNF slurry (3 g, 1 wt%) were uniformly mixed with ultrasonication for 60 min. Subsequently, the mixture was transferred to a Teflon-lined autoclave and heated at 180 °C for 12 h to synthesize a cellulose nanofiber/graphene hydrogel (CGH). Finally, a cellulose nanofiber/graphene aerogel was obtained after freeze-drying and carbonization, and was named as CGA-1:1 (CGA-180 °C). The preparation conditions of each aerogel are shown in Table 1. For comparison, graphene aerogel (GA) was prepared directly from GO. The GO (2 mg/mL, 15 mL) was transferred to a Teflon-lined autoclave and heated at 180 °C for 12 h to synthesize the graphene hydrogel. Finally, the graphene aerogel was obtained after freeze-drying and carbonization, and was named as GA.

Table 1. Preparation of Aerogels at Different Temperatures and Ratios

	Temperature (°C)	Ratio of CNF and GO
CGA-120 °C	120	1:1
CGA-150 °C	150	
CGA-180 °C	180	
CGA-210 °C	210	
GA	180	0:1
CGA-1:2		1:2
CGA-1:1		1:1
CGA-2:1		2:1

Methods

A Nanoscope IIIa atomic force microscope (Veeco Instruments Inc., Plainview, NY, USA) was used to characterize the morphology and size images of graphene oxide and nanocellulose. In the sample preparation, a drop of the diluted graphene oxide or cellulose solution was dispersed on the surface of an optical glass substrate, allowed to dry at ambient temperature, and then analyzed. The microstructure and morphology of samples were observed with a scanning electron microscope (SEM, Hitachi S-4800; Hitachi, Tokyo, Japan). X-ray diffraction (XRD) patterns were measured on an Ultima IV multipurpose X-ray diffraction system (Rigaku, Tokyo, Japan) with CuKα radiation (40 kV and 30 mA) at a scanning rate of 5°/min. Nitrogen adsorption–desorption isotherm measurements were performed using a 3H-2000PS2 Brunauer-Emmett-Teller (BET) surface area analyzer (Yima Optoelec Co., Ltd, Xi'an, China). The pore size distribution of samples was estimated by the Barret–Joyner–Halenda (BJH) method.

Electrochemical Measurements

The electrochemical performances were evaluated by a CHI760e electrochemical workstation (Shanghai Chenhua Instrument Co., Ltd., Shanghai, China) using a two-electrode system in 1 M H_2SO_4 electrolyte solution. The prepared aerogels were cut into pieces with a thickness of 2 mm and directly used as the working electrode. Cyclic voltammetry (CV) measurements were recorded over the potential range of 0 V to 1 V at different scan rates ranging from 5 mV/s to 100 mV/s. Galvanostatic charge-discharge (GCD) tests were conducted in the potential range of 0 V to 1 V at current densities of 0.2 A/g, 0.3 A/g, 0.5 A/g, 1 A/g, and 2 A/g. Electrochemical impedance spectroscopy (EIS) curves were detected at a frequency range of 10 mHz to 100 KHz and the oscillation potential amplitude of 10 mV. Moreover, the specific capacitance (C_s) was calculated based on the CV curves according to the following equation (Wen *et al.* 2016),

$$C_s = \frac{\int I(V)\,\mathrm{d}V}{\mathrm{m}\,v\,\Delta V} \quad (1)$$

where I is the current density applied (A), ΔV is the applied voltage (V), v is the scan rate (mV/s), and m is the mass of the electroactive material in the working electrode (g).

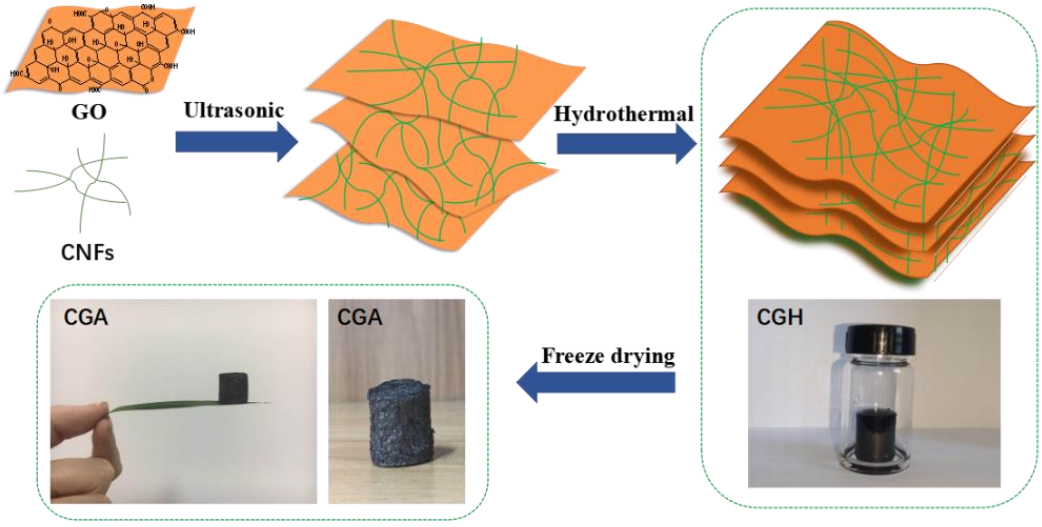

Fig. 1. Schematic illustration of the formation process of CGA

RESULTS AND DISCUSSION

Characterizations

Figures 2a and 2b are atomic force micrographs (AFM) of GO and CNF, respectively. Figure 2a shows that the graphene oxide was uniformly dispersed in the liquid, and the thickness of the single-layer GO was measured as 1.28 nm. Figure 1b shows that the CNF prepared by the TEMPO oxidation method had an interlaced network structure, and the width of the single elongated fiber was approximately 2 nm to 3 nm.

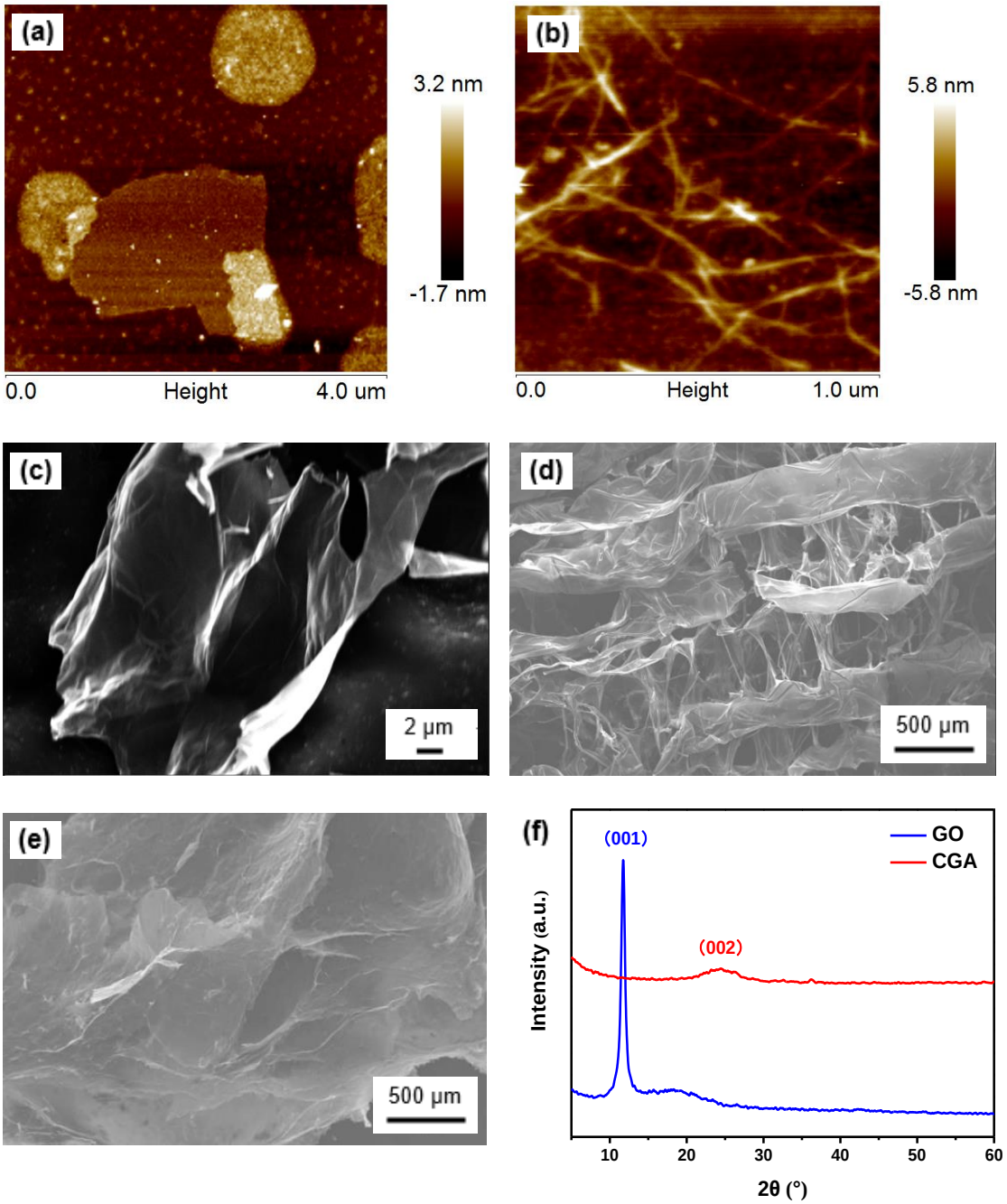

Fig. 2. AFM images of (a) GO and (b) CNFs; SEM images of (c) GO, (d) CNF aerogel, and (e) CGA; (f) XRD of GO and CGA

Figures 1c to 1e show the morphology and microstructure of GO, CNF aerogel, and CGA through the SEM. Figure 2c shows a thin single layer of GO sheet and a smooth surface (Hao *et al.* 2015). The CNF aerogel in Fig. 2d shows a 3D network-like nanostructure and many interconnected pores. The SEM image of the CGA composite electrode (Fig. 2e) shows that CNF and GO crosslinked to form a layered, interconnected porous structure with an ultra-high porosity that facilitated the electrolyte entering the interior of the electrode during the electrochemical reaction. In this process, CNF helped to reduce the aggregation of graphene sheets and bridged GO to form a cross-linked 3D loose structure, thereby promoting the rapid diffusion of electrolyte ions (Suktha *et al.* 2015). Figure 1f shows the typical XRD patterns of GO and CGA, which demonstrated the structural differences between the two samples. Figure 1f shows that the peak in the GO pattern at $2\theta = 11.83°$ corresponded to the characteristic peak (001) reflection of GO. And the CGA composite only showed a broad and low-intensity diffraction peak at $2\theta = 24.54°$, which corresponded to the (002) diffraction peak of graphene, indicating that GO has been converted into graphene by hydrothermal treatment (Sui *et al.* 2015).

Table 2. Pore Structure Characteristics

Sample ID	S_{BET} (m^2/g)	V_{tot} (m^3/g)	W_p (nm)
GA	25.00	0.11	18.35
CNF	8.56	0.04	19.86
CGA	17.71	0.08	17.93

S_{BET} is the specific surface area, V_{tot} is the total pore volume ($P/P_0 = 0.99768871$, pore diameter < 832.8 nm), and W_p is the adsorption average pore size.

Figure 3 shows the pore size distribution and nitrogen isotherm adsorption curves obtained by the BJH method. Figure 2 shows that the pore sizes of GA, CNF aerogel, and CGA were mainly distributed at 2 nm to 10 nm, which indicated that there were mesopores in these three samples, but there were no micropores detected. The maximum pore diameters of GA, CNF, and CGA were 3.15 nm, 2.93 nm, and 3.61 nm, respectively. Table 2 shows the pore structure characteristics of GA, CNF aerogel, and CGA. Table 2 shows that the specific surface areas of the GA, CNF aerogel, and CGA electrode were 25.00 m^2/g, 8.56 m^2/g, and 17.71 m^2/g, respectively.

As can be seen from Fig. 3, the pore size distribution of GA was the most uneven, which can be attributed to the agglomeration of graphene. Therefore, although the specific surface area of GA was relatively high, the uneven dispersion problem of the internal pore size was not conducive to the diffusion of electrolyte ions, which may affect its electrochemical performance. However, compared with GA, the pore size distribution of CGA was more uniform, indicating that CNF as a skeleton, which plays a good supporting role, avoided the aggregation of graphene sheets and forms a good three-dimensional network structure, which was beneficial to the cycle performance of the electrode. At the same time, CNF has good hydrophilicity, which helps to absorb electrolyte ions and provides an effective ion transport route, which is beneficial to the specific capacitance of CGA electrodes.

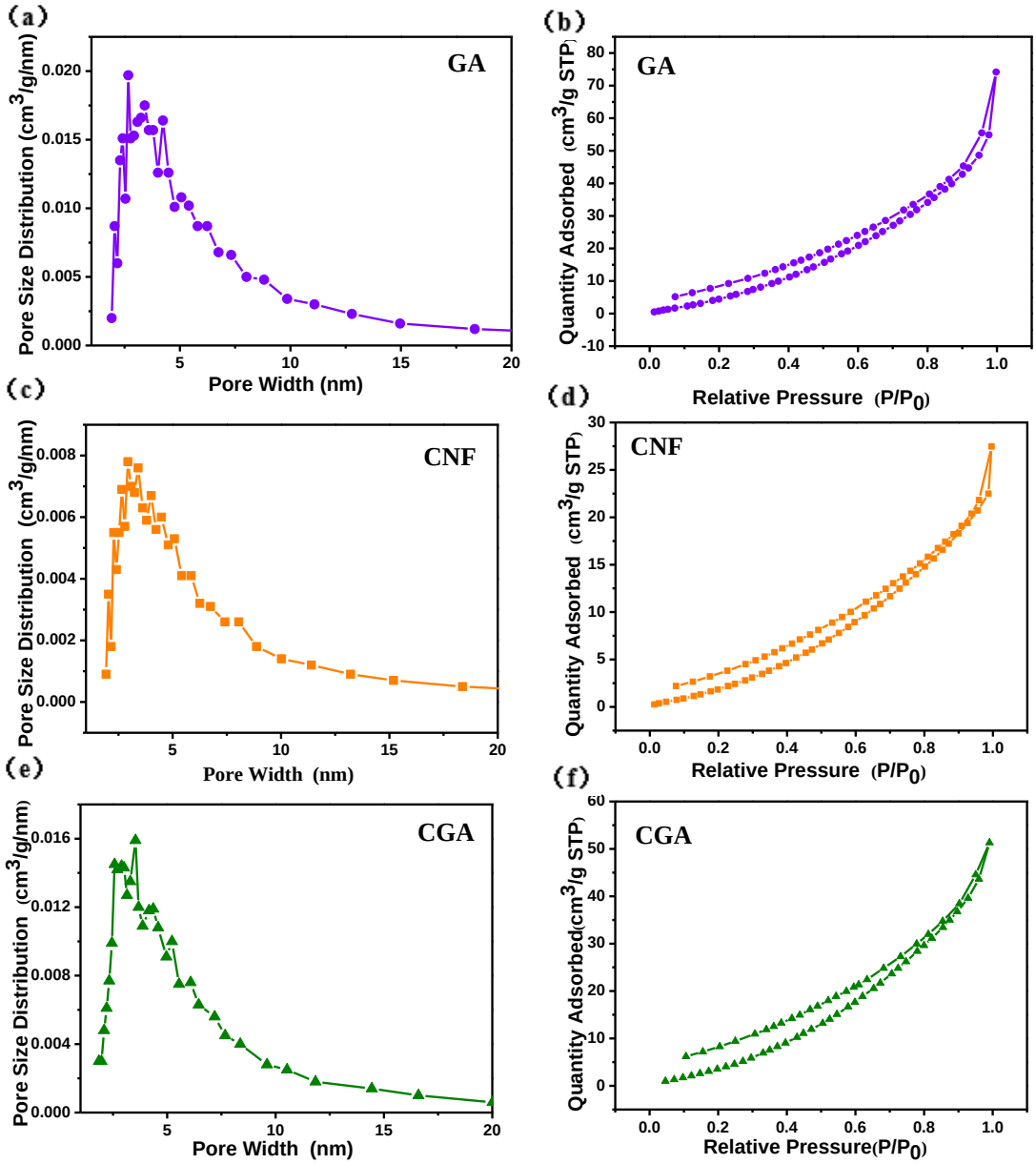

Fig. 3. Pore size distribution of (a) GA, (c) CNF, and (e) CGA; the nitrogen adsorption/desorption isotherms of (b) GA, (d) CNF, and (f) CGA

Electrochemical Performances of CGA Electrodes at Different Temperatures and Ratios

In a two-electrode system, cyclic voltammetry (CV), constant current charge and discharge (GCD), and electrochemical impedance spectroscopy (EIS) were performed on the symmetric capacitor assembled from these electrodes to investigate the effect of electrochemical performances of CGA electrodes at different temperatures (Figs. 4a to 4c) and ratios (Figs. 4d to 4f). The aerogel electrodes prepared under different temperature conditions were recorded as CGA-120 °C, CGA-150 °C, CGA-180 °C, and CGA-210 °C. Similarly, as-prepared aerogel electrodes were recorded as GA, CGA-1:2, CGA-1:1, and CGA-2:1 according to the mass ratio of nanocellulose and graphene.

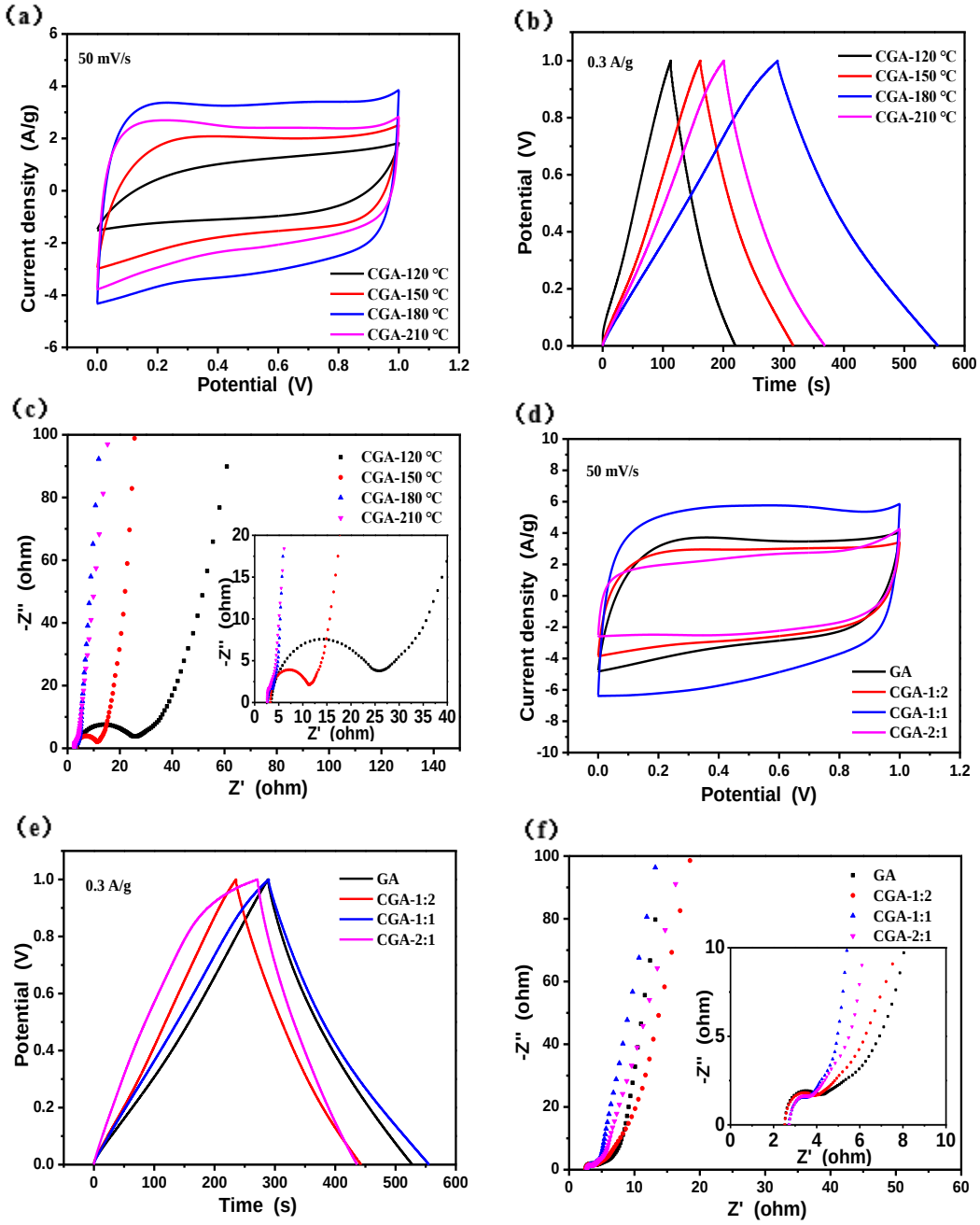

Fig. 4. CGA electrodes at different temperatures: (a) CV curves measured at the scan rate of 50 mV/s, (b) the GCD curves at a current density of 0.3 A/g, (c) Nyquist plots, inset shows the magnified high-frequency regions; CGA electrodes at different ratios: (d) CV curves measured at the scan rate of 50 mV/s, (e) the GCD curves at a current density of 0.3 A/g, and (f) Nyquist plots, inset shows the magnified high-frequency regions

Figure 4a shows the CV curves of CGA electrodes prepared under different temperatures at a scan rate of 50 mV/s. The CV curves of CGA-120 °C, CGA-150 °C, CGA-180 °C, and CGA-210 °C showed nearly rectangular shape, which indicated the ideal electric double layer capacitance (EDLC) behavior of the samples (Yan *et al.* 2014). Notably, CGA-180 °C had the largest integrated area of the CV curve, which meant that CGA-180°C had a better capacitance performance than the other three CGA electrodes.

The GCD curve of the CGA electrodes prepared under different temperatures was measured at the current density of 0.3 A/g (Fig. 4b). All GCD curves exhibited a shape close to the ideal isosceles triangle without a noticeable voltage drop (IR), which indicated that these CGA electrodes had excellent capacitance performance. The CGA-180 °C had the longest time to complete a charge-discharge process, which indicated that 180 °C was the most suitable temperature for preparing CGA electrodes.

The Nyquist plot in Figure 4c was used to analyze the electrochemical transfer properties of the CGA electrodes. The equivalent series resistance (ESR) of CGA-180 °C (3.1 Ω) was smaller than other CGA electrodes, showing better capacitive characteristics than other CGA electrodes. The Nyquist plot was close to a semi-arc shape in the high frequency region, which showed the charge transfer process at the interface between the active ingredient and the electrolyte. The semicircle of CGA-180 °C in the high frequency region was the smallest, which indicated that the charge transfer resistance (R_{ct}) was the lowest. Similarly, Fig. 4c clearly shows that the Nyquist plot of CGA-180 °C at the low frequency region was the most vertical, which indicated that the CGA-180 °C had better capacitive characteristics than other CGA electrodes.

Figure 4d shows the CV curves of the GA, CGA-1:2, CGA-1:1, and CGA-2:1 electrodes at a scan rate of 50 mV/s. The CGA-1:1 curve shape was closer to a big rectangle than the CGA-1:2, CGA-2:1, and GA, which was an ideal electrical double layer capacitor. Figure 4e shows the GCD curve of the CGA electrode at a current density of 0.3 A/g. The GCD curves of GA, CGA-2:1, CGA-1:1, and CGA-1:2 were linear, exhibiting a typical triangle, which indicated good electrochemical capacitance characteristics. The CGA-1:1 electrode needed the longest time to complete a charge-discharge cycle. Among these electrodes, the Nyquist curve (Fig. 4f) of the CGA1:1 electrode exhibited a minimum semicircle diameter in the high frequency region, indicating that the charge transfer resistance (R_{ct}) was the lowest, and the curve in the low frequency region was the most perpendicular to the Z' axis, indicating good ion diffusion rate and excellent adsorption performance on the electrode surface.

Electrochemical Performances of CGA Electrode

Figure 5a shows that the rectangular area of the CGA (prepared under the temperature of 180 °C and 1:1 ratio of GO and CNF) increased with increasing scan rate from 5 mV/s to 100 mV/s in 1 M H_2SO_4 electrolyte, which indicated that CGA electrode had a good rate performance (Du *et al.* 2014). All of the GCD curves at different current densities are shown in Fig. 5b. All curves had a nearly linear slope and an almost symmetrical isosceles triangle shape, which indicated a fast current-voltage response and high power transfer efficiency of the CGA electrode (Jeong *et al.* 2011). The specific capacitance of the CGA electrode was calculated from the CV curve at different scan rates as shown in Fig. 5c. The specific capacitance of CGA was 125.22 F/g, 122.71 F/g, 118.08 F/g, 110.54 F/g, and 101.78 F/g when the scanning rates were 5 mV/s, 10 mV/s, 20 mV/s, 50 mV/s, and 100 mV/s, respectively. As the scan rate was increased from 5 mV/s to 100 mV/s, the specific capacitance was only reduced 23.44 F/g, and the capacitance retention rate was as high as 81.28%. The excellent cycle stability of the supercapacitors can play an important role in practical applications. Figure 5d shows the capacitance retention of the CGA electrode after 5000 cycles of continuous charging and discharging. The inset shows the GCD curve of the CGA electrode after 5000 cycles of continuous charging and discharging at a current density of 2 A/g. The GCD curve of the CGA electrode maintained the original isosceles triangle after 5000 cycles of charge and

discharge, and the capacitance retention rate was 98.3%, which indicated that the CGA electrode had excellent long-term electrochemical stability. Compared with other composite electrodes (Table 3.), the CGA electrode exhibited both high specific capacitance and good electrochemical stability.

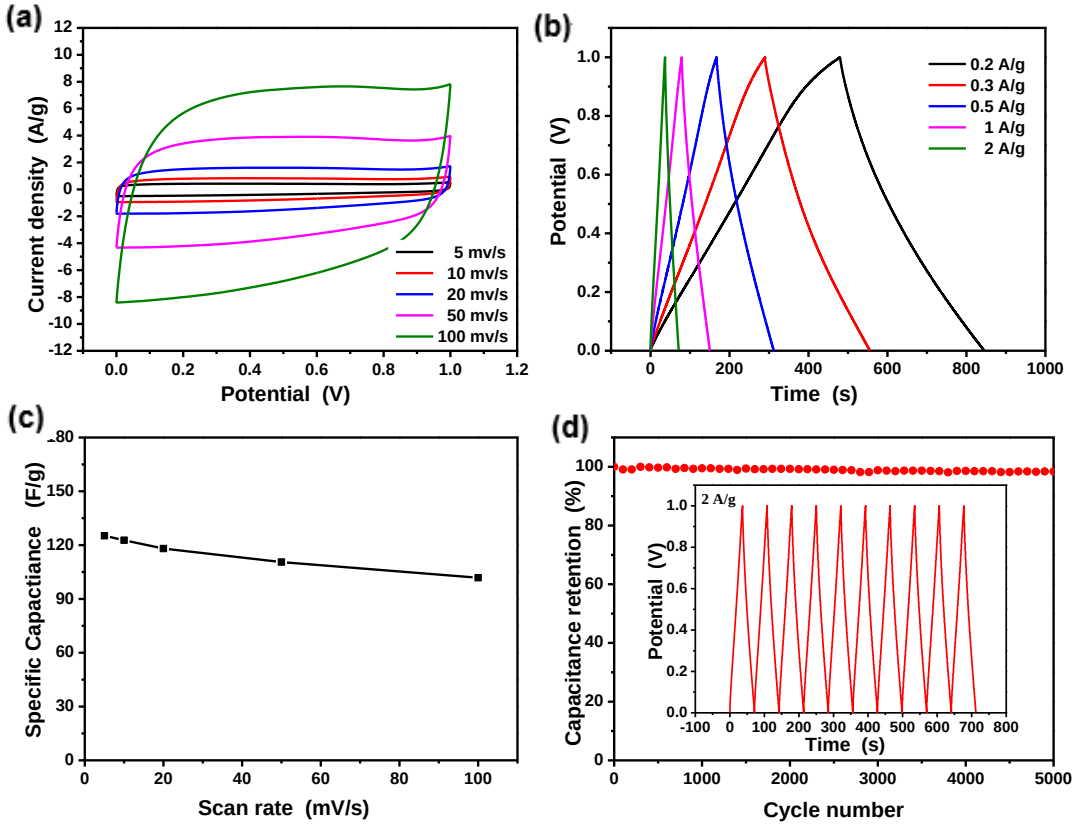

Fig. 5. (a) CV curves of CGA electrode at different scan rates, (b) GCD curves of CGA electrode at different current densities, (c) specific capacitances of CGA electrode at different scan rate, and (d) cycling performance of the CGA electrode at 2 A/g

Table 3. Specific capacitance of different composite electrodes

Composite electrodes	Specific capacitances	Cycling Performance	References
CGA	125.5 $F \cdot g^{-1}$, $5mV \cdot s^{-1}$	98.3%, 5000 cycles at $2A \cdot g^{-1}$	This work
Graphene/Cellulose	120 $F \cdot g^{-1}$, 1 $mV \cdot s^{-1}$	99%, 5000 cycles at 50 $mV \cdot s^{-1}$	(Weng *et al.* 2011)
3D holey MnO_2/HGO	117.45 $F \cdot g^{-1}$, 5 $mV \cdot s^{-1}$	N/A	(Wang *et al.* 2015)
rGO/PPy hybrid paper	440 $mF \cdot cm^{-1}$, 0.5 $A \cdot g^{-1}$	81%, 1000 cycles at $6A \cdot g^{-1}$	(Shu *et al.* 2016)
PANI/BC/ Graphene paper	6.15 $F \cdot cm^{-1}$, 1 $mA \cdot cm^{-2}$	56.3%, 8000 cycles at 50 $mA \cdot cm^{-2}$	(Liu *et al.* 2016)
RGO/PPy/CCFs	122.7 $F \cdot g^{-1}$, 20 $mV \cdot s^{-1}$	84%, 600 cycles at 20 $mV \cdot s^{-1}$	(Lyu *et al.* 2016)

CONCLUSIONS

1. Graphene oxide (GO) and cellulose nanofibers (CNF) were used as starting materials, and low-cost CGA electrodes were successfully prepared by simple hydrothermal method and hydrothermal process optimization. The porous structure of the CGA electrode provided more effective delivery routes for ions during charge and discharge.
2. The specific surface area and maximum pore diameter of the CGA electrode were 17.71 m^2 /g and 3.61 nm, respectively. The CGA electrode used CNF as the carrier, and the cross-linking with GO increased the specific surface area of the aerogel, which could be better used as an electrolyte reservoir.
3. The symmetric capacitor assembled from the CGA electrode exhibited excellent double-layer capacitance performance with a high specific capacitance of 125.5 F/g at the scan rate of 5 mV/s. The specific capacitance retention of the CGA electrode was 98.3% after 5000 cycles.

ACKNOWLEDGMENTS

The authors completed this work with financial support from the National Key R&D Program of China (Grant No. 2017YFD0600804).

REFERENCES CITED

Chen, W., Yu, H., Lee, S.-Y., Wei, T., Li, J., and Fan, Z. (2018). "Nanocellulose: A promising nanomaterial for advanced electrochemical energy storage," *Chem. Soc. Rev.* 47(8), 2837-2872. DOI: 10.1039/C7CS00790F

Chen, W., Yu, H., and Liu, Y. (2011). "Preparation of millimeter-long cellulose I nanofibers with diameters of 30–80 nm from bamboo fibers," *Carbohyd. Polym.* 86(2), 453-461. DOI: 10.1016/j.carbpol.2011.04.061

Du, W., Qi, S., Zhou, B., Sun, P., Zhu, L., and Jiang, X. (2014). "A surfactant-free water-processable all-carbon composite and its application to supercapacitor," *Electrochim. Acta* 146, 353-358. DOI: 10.1016/j.electacta.2014.09.030

Du, X., Zhang, Z., Liu, W., and Deng, Y. (2017). "Nanocellulose-based conductive materials and their emerging applications in energy devices - A review," *Nano Energy* 35, 299-320. DOI: 10.1016/j.nanoen.2017.04.001

Dufresne, A. (2013). "Nanocellulose: A new ageless bionanomaterial," *Mater. Today* 16(6), 220-227. DOI: 10.1016/j.mattod.2013.06.004

Feng, Y., Zhang, X., Shen, Y., Yoshino, K., and Feng, W. (2012). "A mechanically strong, flexible and conductive film based on bacterial cellulose/graphene nanocomposite," *Carbohyd. Polym.* 87(1), 644-649. DOI: 10.1016/j.carbpol.2011.08.039

Gao, K., Shao, Z., Wu, X., Wang, X., Li, J., Zhang, Y., Wang, W., and Wang, F. (2013). "Cellulose nanofibers/reduced graphene oxide flexible transparent conductive paper," *Carbohyd. Polym.* 97(1), 243-251. DOI: 10.1016/j.carbpol.2013.03.067

González, A., Goikolea, E., Barrena, J.A., and Mysyk, R. (2016). "Review on supercapacitors: Technologies and materials," *Renew. Sust. Energ. Rev.* 58, 1189-1206. DOI: 10.1016/j.rser.2015.12.249

Gryglewicz, G., Śliwak, A., and Béguin, F. (2013). "Carbon nanofibers grafted on activated carbon as an electrode in high-power supercapacitors," *ChemSusChem* 6(8), 1516-1522. DOI: 10.1002/cssc.201300095

Hao, P., Zhao, Z., Leng, Y., Tian, J., Sang, Y., Boughton, R.I., Wong, C., Liu, H., and Yang, B. (2015). "Graphene-based nitrogen self-doped hierarchical porous carbon aerogels derived from chitosan for high performance supercapacitors," *Nano Energy* 15, 9-23. DOI: 10.1016/j.nanoen.2015.02.035

Hummers Jr, W. S., and Offeman, R. E. (1958). "Preparation of graphitic oxide," *J. Am. Chem. Soc.* 80(6), 1339-1339. DOI: 10.1021/ja01539a017

Isogai, A., Saito, T., and Fukuzumi, H. (2011). "TEMPO-oxidized cellulose nanofibers," *Nanoscale* 3(1), 71-85. DOI: 10.1039/c0nr00583e

Izadi-Najafabadi, A., Yasuda, S., Kobashi, K., Yamada, T., Futaba, D.N., Hatori, H., Yumura, M., Iijima, S., and Hata, K. (2010). "Extracting the full potential of single-walled carbon nanotubes as durable supercapacitor electrodes operable at 4 V with high power and energy density," *Adv. Mater.* 22(35), E235-E241. DOI: 10.1002/adma.200904349

Jeong, H. M., Lee, J. W., Shin, W. H., Choi, Y. J., Shin, H. J., Kang, J. K., and Choi, J. W. (2011). "Nitrogen-doped graphene for high-performance ultracapacitors and the importance of nitrogen-doped sites at basal planes," *Nano Lett.* 11(6), 2472-2477. DOI: 10.1021/nl2009058

Lei, Z., Zhang, J., Zhang, L. L., Kumar, N. A., and Zhao, X. (2016). "Functionalization of chemically derived graphene for improving its electrocapacitive energy storage properties," *Energ. Environ. Sci.* 9(6), 1891-1930. DOI: 10.1039/c6ee00158k

Li, Z., Liu, J., Jiang, K., and Thundat, T. (2016). "Carbonized nanocellulose sustainably boosts the performance of activated carbon in ionic liquid supercapacitors," *Nano Energy* 25, 161-169. DOI: 10.1016/j.nanoen.2016.04.036

Liu, R., Ma, L., Huang, S., Mei, J., Xu, J., and Yuan, G. (2016). "Large areal mass, flexible and freestanding polyaniline/bacterial cellulose/graphene film for high-performance supercapacitors," *RSC Adv.* 6(109), 107426-107432. DOI: 10.1039/C6RA21920A

Lyu, S., Chang, H., Fu, F., Hu, L., Huang, J., and Wang, S. (2016). "Cellulose-coupled graphene/polypyrrole composite electrodes containing conducting networks built by carbon fibers as wearable supercapacitors with excellent foldability and tailorability," *J Power Sources* 327, 438-446. DOI: 10.1016/j.jpowsour.2016.07.091

Merlet, C., Rotenberg, B., Madden, P.A., Taberna, P.-L., Simon, P., Gogotsi, Y., and Salanne, M. (2012). "On the molecular origin of supercapacitance in nanoporous carbon electrodes," *Nat. Mater.* 11(4), 306. DOI: 10.1038/nmat3260

Okita, Y., Saito, T., and Isogai, A. (2010). "Entire surface oxidation of various cellulose microfibrils by TEMPO-mediated oxidation," *Biomacromolecules* 11(6), 1696-1700. DOI: 10.1021/bm100214b

Park, M., Lee, D., Shin, S., Kim, H.J., and Hyun, J. (2016). "Flexible conductive nanocellulose combined with silicon nanoparticles and polyaniline," *Carbohydr Polym*. 140, 43-50. DOI: 10.1016/j.carbpol.2015.12.046

Saeed, G., Kumar, S., Kim, N. H., and Lee, J. H. (2018). "Fabrication of 3D graphene-CNTs/α-MoO3 hybrid film as an advance electrode material for asymmetric supercapacitor with excellent energy density and cycling life," *Chem. Eng. J.* 352, 268-276. DOI: 10.1016/j.cej.2018.07.026

Saito, T., Nishiyama, Y., Putaux, J.-L., Vignon, M., and Isogai, A. (2006). "Homogeneous suspensions of individualized microfibrils from TEMPO-catalyzed oxidation of native cellulose," *Biomacromolecules* 7(6), 1687-1691. DOI: 10.1021/bm060154s

Shu, K., Wang, C., Zhao, C., Ge, Y., and Wallace, G.G. (2016). "A free-standing graphene-polypyrrole hybrid paper via electropolymerization with an enhanced areal capacitance," *Electrochim Acta* 212, 561-571. DOI: 10.1016/j.electacta.2016.07.052

Sui, Z.-Y., Meng, Y.-N., Xiao, P.-W., Zhao, Z.-Q., Wei, Z.-X., and Han, B.-H. (2015). "Nitrogen-doped graphene aerogels as efficient supercapacitor electrodes and gas adsorbents," *ACS Appl. Mater. Inter.* 7(3), 1431-1438. DOI: 10.1021/am5042065

Suktha, P., Chiochan, P., Iamprasertkun, P., Wutthiprom, J., Phattharasupakun, N., Suksomboon, M., Kaewsongpol, T., Sirisinudomkit, P., Pettong, T., and Sawangphruk, M. (2015). "High-performance supercapacitor of functionalized carbon fiber paper with high surface ionic and bulk electronic conductivity: Effect of organic functional groups," *Electrochim. Acta* 176, 504-513. DOI: 10.1016/j.electacta.2015.07.044

Sun, G., Li, K., Xie, L., Wang, J., and Li, Y. (2012). "Preparation of mesoporous carbon spheres with a bimodal pore size distribution and its application for electrochemical double layer capacitors based on ionic liquid as the electrolyte," *Micropor. Mesopor. Mater.* 151, 282-286. DOI: 10.1016/j.micromeso.2011.10.023

Titirici, M.-M., White, R. J., Falco, C., and Sevilla, M. (2012). "Black perspectives for a green future: Hydrothermal carbons for environment protection and energy storage," *Energ. Environ. Sci.* 5(5), 6796-6822. DOI: 10.1039/C2EE21166A

Wang, H., Bian, L., Zhou, P., Tang, J., and Tang, W. (2013). "Core–sheath structured bacterial cellulose/polypyrrole nanocomposites with excellent conductivity as supercapacitors," *J. Mater. Chem. A* 1(3), 578-584. DOI: 10.1039/C2TA00040G

Wang, L., Deng, D., Salley, S. O., and Ng, K. S. (2015). "Facile synthesis of 3-D composites of MnO_2 nanorods and holey graphene oxide for supercapacitors," *J. Mater. Sci.* 50(19), 6313-6320. DOI: 10.1007/s10853-015-9169-8

Wen, J., Li, S., Zhou, K., Song, Z., Li, B., Chen, Z., Chen, T., Guo, Y., and Fang, G. (2016). "Flexible coaxial-type fiber solid-state asymmetrical supercapacitor based on Ni_3S_2 nanorod array and pen ink electrodes," *J. Power Sources* 324, 325-333. DOI: 10.1016/j.jpowsour.2016.05.087

Weng, Z., Su, Y., Wang, D. W., Li, F., Du, J., and Cheng, H. M. (2011). "Graphene–cellulose paper flexible supercapacitors," *Adv Energy Mater* 1(5), 917-922. DOI:org/10.1002/aenm.201100312

Wu, X., Tang, J., Duan, Y., Yu, A., Berry, R. M., and Tam, K. C. (2014). "Conductive cellulose nanocrystals with high cycling stability for supercapacitor applications," *J. Mater. Chem. A* 2(45), 19268-19274. DOI: 10.1039/C4TA04929B

Xu, Y., Chen, C.-Y., Zhao, Z., Lin, Z., Lee, C., Xu, X., Wang, C., Huang, Y., Shakir, M. I., and Duan, X. (2015). "Solution processable holey graphene oxide and its derived

macrostructures for high-performance supercapacitors," *Nano Lett.* 15(7), 4605-4610. DOI: 10.1021/acs.nanolett.5b01212

Yan, J., Wang, Q., Wei, T., Jiang, L., Zhang, M., Jing, X., and Fan, Z. (2014). "Template-assisted low temperature synthesis of functionalized graphene for ultrahigh volumetric performance supercapacitors," *ACS Nano* 8(5), 4720-4729. DOI: 10.1021/nn500497k

Yu, S., Li, Y., and Pan, N. (2014). "KOH activated carbon/graphene nanosheets composites as high performance electrode materials in supercapacitors," *RSC Adv.* 4(90), 48758-48764. DOI: 10.1039/c4ra06710j

Zhang, H., Dou, C., Pal, L., and Hubbe, M. A. (2019). "Review of electrically conductive composites and films containing cellulosic fibers or nanocellulose," *BioResources* 14(3), 7494-7542.

Zhou, T., Chen, D., Jiu, J., Nge, T.T., Sugahara, T., Nagao, S., Koga, H., Nogi, M., Suganuma, K., Wang, X., Liu, X., Cheng, P., Wang, T., and Xiong, D. (2013). "Electrically conductive bacterial cellulose composite membranes produced by the incorporation of graphite nanoplatelets in pristine bacterial cellulose membranes," *Express Polym Lett* 7(9), 756-766. DOI: 10.3144/expresspolymlett.2013.73

Zhu, Y., Murali, S., Stoller, M. D., Ganesh, K., Cai, W., Ferreira, P. J., Pirkle, A., Wallace, R. M., Cychosz, K. A., and Thommes, M. (2011). "Carbon-based supercapacitors produced by activation of graphene," *Science* 332(6037), 1537-1541. DOI: 10.1126/science.1200770

Article submitted: September 12, 2019; Peer review completed: November 17, 2019; Revised version received and accepted: November 24, 2019; Published: December 4, 2019.
DOI: 10.15376/biores.15.1.677-690